J Therm Anal Calorim (2011) 105:171–186
DOI 10.1007/s10973-011-1512-y

Estimation of cracking risk of concrete at early age based on thermal stress analysis

Shengxing Wu · Donghui Huang · Feng-Bao Lin · Haitao Zhao · Panxiu Wang

Received: 22 December 2010 / Accepted: 17 March 2011 / Published online: 5 April 2011

Abstract The purpose of this study is to simulate the early age concrete behaviors and evaluate the cracking risk with the thermal and thermal stress analysis. A new finite element method program associated with ANSYS program is developed for the computation of thermal field and thermal stress field for early age concrete considering the following characters: degree of hydration, thermal properties (such as specific heat, thermal diffusivity), thermal boundary conditions, and mechanical properties (such as shrinkage, creep) which occur at early age. The results from simulation compared with experimental values found in the literature show a good agreement. Finally, based on this user-developed subroutine, the effects of hydration heat, ambient temperature, wind velocity, shrinkage, and length-height ratio on cracking risk were analyzed for a concrete wall which is one part of the structure of Maridal culvert in Norway. By which, the measures to control the cracking were provided for the engineering application.

Keywords Concrete · Early age · Thermal stress · Cracking risk · Finite element method

S. Wu · D. Huang · H. Zhao (✉) · P. Wang
Hohai University, 1 Xikang Road, 210098 Nanjing, China
e-mail: hhuzhaoht@163.com

S. Wu
e-mail: sxwu@hhu.edu.cn

D. Huang
e-mail: cehhu@hotmail.com

P. Wang
e-mail: wpanxiu@hotmail.com

F.-B. Lin
City College of New York, 160 Convent Avenue, New York, NY 10031, US
e-mail: flin@ccny.cuny.edu

Introduction

Cracking in the early age concrete often results from restrained volume changes due to temperature change during the hydration. Cracking may reduce the concrete durability against aggressive substance as well as increased risk of corrosion in reinforcement bars [1]. It is well known that the heat of hydration [2] is the inner ingredient of cracking propagation induced by the internal and external restrains under non-uniform temperature distribution across the concrete mass. Besides, the environmental conditions have effects on the temperature distribution of the concrete. Solar radiation may also cause more harmful internal stresses due to the rapid variation of thermal boundary. On the other hand, creep and shrinkage, which result in complex deformation of early age concrete, have important influences on the development of thermal stress.

Many numerical models have been developed for comprehending and predicting the concrete creep and shrinkage behavior at early age [3–9]. ACI proposed a report for prediction of creep, shrinkage, and temperature effects in concrete structures. The analysis method was given regarding the creep, shrinkage, temperature, and related parameter value [10]. Improved Production of Advanced Concrete Structures (IPACS) reported stress predictions in hardening concrete for avoiding the premature cracking. It took material properties as the function of microstructural parameters and creep as a function of maturity [11]. Borst and Boogaard [12] studied deformation and cracking in early age concrete modeled by finite element method considering hardening process of young concrete, heat production, stiffness evolution, and concrete creep. The numerical model of the solar radiation has been widely used in the engineering application [13, 14].

For estimation of the cracking behavior of early age concrete, the following concrete properties must be considered in a correct way including heat of hydration, thermal conductivity, heat transfer coefficient, specific heat, coefficient of thermal expansion, thermal boundary conditions, shrinkage, creep, and development of elastic modulus and tensile strength.

In this article, based on a transient heat conduction analysis of the concrete structure, the numerical strategies are implemented considering the cement hydration, creep, shrinkage, and solar radiation for early age concrete. The objective is to document and hopefully verify a method of thermal analysis and describe cracking risk estimation, where the effect of structural restraint caused by adjoining structures and non-uniform temperature distribution are included. The main studies of this article are shown as follows. (1) Develop the subroutines of the creep and shrinkage for the early age concrete based on the FEM software ANSYS program with its User-Programmable Features (UPFs). (2) Introduce the mathematical model of solar radiation into the simulation of early age concrete structures with modified thermal boundary conditions, and develop a subroutine to calculate the solar radiation. (3) Analyze the probability of cracking risk by the developed program, by which some reasonable advices are provided to control the cracking risk.

Mathematic models

Degree of hydration and adiabatic temperature rise model

The hydration process is generally represented by the degree of hydration which can be expressed as the ratio of current liberated heat of hydration to ultimate liberated heat of hydration [15–17]:

$$\alpha(t) = \frac{Q(t)}{Q_u} \tag{1}$$

where $\alpha(t)$ is the degree of hydration at time t, $Q(t)$ is cumulative heat of hydration released at time t (kJ kg^{-1}), and Q_u is total ultimate heat of hydration of concrete (kJ kg^{-1}).

Assuming that the specific heat of concrete is a constant (actually it varies within a little range [6]) during the hydration process, the relationship between adiabatic temperature rise and cumulative released heat of hydration is given by:

$$Q(t) = c\theta(t) \tag{2}$$

where $\theta(t)$ is adiabatic temperature rise by time t (°C), and c is specific heat (kJ kg^{-1} °C).

Thus, the degree of hydration can also be simplified and expressed as:

$$\alpha(t) = \frac{\theta(t)}{\theta_u} \tag{3}$$

where θ_u is the ultimate adiabatic temperature rise (°C).

The maturity method is a technique to account for the combined effects of time and temperature on the strength development of concrete. Freiesleben Hansen and Pedersen [18] proposed a new formulation based on the Arrhenius equation which was used to describe the effect of temperature on the rate of a chemical reaction [19, 20]. In this formulation, the equivalent age of concrete is first computed as follows:

$$t_e = \sum_0^t \exp\left[\frac{E_a}{R}\left(\frac{1}{293} - \frac{1}{273+T}\right)\right]\Delta t \tag{4}$$

where t_e is the equivalent age of concrete at the reference temperature, E_a is the apparent activation energy generally varying from 25000 to 40000 (J mol^{-1}), R is the universal gas constant which is equal to 8.314 (J mol^{-1} K), and T is the average value of actual temperature of concrete during interval Δt (°C).

Based on experimental investigations, several mathematical models were proposed for the relationship between degree of hydration and equivalent age [21–23]. In the current study, the following expression is adopted [24, 25]:

$$\alpha(t_e) = \alpha_u(1 - \exp(-\xi t_e)) \tag{5}$$

where α_u is the ultimate degree of hydration, and ξ is a constant determined by the experiments. Similarly, the formula for the adiabatic temperature rise based on the maturity of the equivalent age can be expressed as follows [7]:

$$\theta(t_e) = \theta_u(1 - \exp(-\xi t_e)) \tag{6}$$

Thermal properties

Specific heat and thermal conductivity

It was concluded based on the experimental results that the specific heat as well as the thermal diffusivity proportionally decreases with increasing degree of hydration of concrete. For a conventional gravel concrete, the following relations may apply [6]:

$$\begin{aligned} c(\alpha) &= c_0(1.15 - 0.15\alpha) \\ k(\alpha) &= k_0(1.10 - 0.10\alpha) \end{aligned} \tag{7}$$

where $c(\alpha)$ is the specific heat of hardening concrete at degree of hydration α (kJ kg^{-1} °C), c_0 is the specific heat of hardened concrete (kJ kg^{-1} °C), $k(\alpha)$ is the thermal

conductivity of hardening concrete at degree of hydration α (W m^{-1} °C), and k_0 is the thermal conductivity of hardened concrete (W m^{-1} °C).

Coefficient of thermal expansion

Some researchers have studied the coefficient of thermal expansion of concrete [26, 27]; however, no reliable formula has been developed related to the degree of hydration or maturity. A constant value for the coefficient of thermal expansion 1×10^{-5} (°C^{-1}) is assumed in this study.

Convection coefficient

Convection heat transfer coefficients for the boundaries can be calculated as follows [28]:

$$h_{\text{free}} = \begin{cases} 5.6 + 3.95\ v & (v \le 5\ \text{m/s}) \\ 7.8\ v^{0.78} & (v > 5\ \text{m/s}) \end{cases} \tag{8}$$

where h_{free} is the convection heat transfer coefficient on the free surface (W m^{-1} °C), and v is the wind velocity (m s^{-1}). If there are formwork or insulation slab covered on the concrete, the integration convection heat transfer coefficient can be calculated by:

$$h_{\text{i}} = \left(\frac{1}{h_{\text{free}}} + \sum \frac{l_i}{k_i} \right)^{-1} \tag{9}$$

where h_{i} is the integration convection heat transfer coefficient considering multi-layer covers on the surface of the concrete structure (W m^{-2} °C), l_{i} is the thickness of the ith layer cover (m), and k_{i} is the conductivity of the ith layer cover (W m^{-1} °C).

Ambient temperature

In this study, a double cosine model consists of three sinusoidal segments [29] represented by:

$$\begin{aligned} T_{\text{air}}(y,\ m,\ d,\ t) &= T_{\text{air}}(y,\ m,\ d) - \frac{A_{\text{T}}(y,\ m,\ d)}{2} \\ &\times \cos\left[\frac{\pi(t_{T\min} - t)}{24 + t_{T\min} - t_{T\max}} \right] \qquad 1 \le t \le t_{T\min} \\ T_{\text{air}}(y,\ m,\ d,\ t) &= T_{\text{air}}(y,\ m,\ d) + \frac{A_{\text{T}}(y,\ m,\ d)}{2} \\ &\times \cos\left[\frac{\pi(t_{T\max} - t)}{24 + t_{T\min} - t_{T\max}} \right] \qquad t_{T\min} < t \le t_{T\max} \\ T_{\text{air}}(y,\ m,\ d,\ t) &= T_{\text{air}}(y,\ m,\ d) - \frac{A_{\text{T}}(y,\ m,\ d)}{2} \\ &\times \cos\left[\frac{\pi(t_{T\min} - t)}{24 + t_{T\min} - t_{T\max}} \right] \qquad t_{T\max} < t \le 24 \end{aligned} \tag{10}$$

where $T_{\text{air}}(y,\ m,\ d,\ t)$ is the hourly mean air temperature (°C), $T_{\text{air}}(y,\ m,\ d)$ is the daily mean air temperature (°C), $A_{\text{T}}(y,\ m,\ d)$ is the daily thermal amplitude (°C), $t_{T\min}$ and $t_{T\max}$ are the hours at which the daily minimum and maximum temperatures occur respectively, t is the hour of the day when the temperature is computed, and y, m, and d are the numbers of year, month, and day, respectively.

Solar radiation

In general, the intensity of solar radiation at an arbitrary time is a function of the surface inclination angle, surface orientation, declination of the sun, solar elevation, hour angle of the sun, and the earth's latitude and longitude [11].

Main parameters involved in solar radiation model

Declination of the sun Declination of the sun can be described mathematically with a very high accuracy in several expressions. The expression adopted in this study is shown as follows [30]:

$$\begin{aligned} \delta = \frac{180}{\pi}(&0.006918 - 0.399912\cos\gamma + 0.070257\sin\gamma \\ &- 0.006758\cos 2\gamma + 0.000907\sin 2\gamma \\ &- 0.002697\cos 3\gamma + 0.00148\sin 3\gamma) \end{aligned} \tag{11}$$

where δ is the declination of the sun expressed in radian, $\gamma = \frac{2\pi}{365}(N-1)$, and N is the number of days in a tropical year ranging from 1 on January 1 to 365 on December 31.

Hour angle of the sun The hour angle of the sun is defined as the actual orientation of the earth with respect to the sun. And it is known that the earth turns 15° further every hour. Thus, the relationship between the local time and the hour angle of the sun is:

$$\Omega = (\text{LAT} - 12) \times 15 \tag{12}$$

where Ω is the hour angle of the sun, and LAT is the local apparent solar time which can be expressed as:

$$\text{LAT} = \text{LST} + \text{Long} + \text{ET} \tag{13}$$

where LST is the local standard time, Long is the longitude east of the standard meridian measured in minutes of time (1° = 4 min of time), and ET is the equation of time in minutes giving a correction from the mean to apparent time.

$$\text{ET} = [-7.655\sin M + 9.873\sin(2M + 3.588)] \tag{14}$$

where $M = \frac{2\pi N}{365.242}$.

Solar elevation angle The solar elevation is defined as the elevation of the sun in degrees observed from the earth surface. The solar elevation can be calculated with a good approximation using the formula:

$$\sin(h) = \sin\varphi \sin\delta + \cos\varphi \cos\delta \cos\Omega \quad (15)$$

where h is the solar elevation angle, and φ is the local latitude.

Solar azimuth angle The solar azimuth angle is defined as the angle between the line from the observer to the sun projected on the ground and the line from the observer due south. It can be calculated using the following formula:

$$\sin(\psi_0) = \cos(\delta)\sin(\Omega)/\cos(h) \quad (16)$$

where ψ_0 is the solar azimuth angle.

However, the angle computed should be interpreted carefully for its sign. A positive azimuth angle indicates that the sun is toward the eastern direction from the south, and a negative value indicates the sun is toward the western direction.

Horizontal global radiation and its components

Based on the clear sky model, European Solar Radiation Atlas (ESRA) developed a model to estimate solar radiation at ground level considering the Linke turbidity factor which is a function of the scattering by aerosols and the absorption by gas (mainly water vapor) [31]. In this model, the horizontal global radiation (G_c) on a surface consists of two parts: the direct component (G_b) and the diffuse component (G_d). The formulas are given by:

$$G_c = G_b + G_d \quad (17)$$

$$G_b = I_0\,\varepsilon\,\sin(h)\exp(-0.8662T_L(AM2)\;m\,\delta_R(m)) \quad (18)$$

$$G_d = I_0\,\varepsilon\,T_{rd}(T_L(AM2))F_d(\gamma_s,\,T_L(AM2)) \quad (19)$$

where I_0 is the solar constant and equal to 1367 (W m^{-2}) which represents the extraterrestrial radiation normal to the solar beam at the mean solar distance, $\varepsilon = 1 + 0.033\cos(2\pi N/365)$ is a correction used to allow for the variation of sun–earth distance from its mean value, h is the solar elevation angle as defined previously, $T_L(AM2)$ is the Linke turbidity factor, $\delta_R(m)$ is the integral Rayleigh optical thickness, T_{rd} is the diffuse transmission function, and F_d is the diffuse angular function. The detailed expressions of these parameters were given by Rigollier [31].

Solar radiation on an inclined surface

With the clear sky model and isotopic model, the slope radiation is developed which assumes that the diffuse radiation is uniformly distributed over the complete sky dome. The total radiation on an inclined surface is the summation of the beam, the diffuse, and the reflected radiations on the surface. It is given [13, 14] as:

$$G_i = G_{b,i} + G_{d,i} + G_{r,i} \quad (20)$$

where G_i, $G_{b,i}$, $G_{d,i}$, $G_{r,i}$ are the total radiation, beam radiation, diffuse radiation, and reflected radiation on an inclined surface, respectively (W m^{-2}). The latter three parameters can be computed by:

$$G_{b,i} = G_b\cos\theta_i/\sin(h), \quad G_{d,i} = G_d(1+\cos\beta)/2,$$
$$G_{r,i} = \rho_g G_c(1-\cos\beta)/2 \quad (21)$$

where θ_i is the angle between the incidence and the normal to the surface which is given by:

$$\cos\theta_i = \cos\beta\sin(h) + \sin\beta\cos(h)\cos(\psi_0 - \psi_n) \quad (22)$$

in which β is the angle of inclination of the surface relative to the horizontal plane, ψ_0 is the solar azimuth, ψ_n is azimuth of projection of the normal to the surface on the horizontal plane, and ρ_g is the average reflectance of the ground.

Sol–Air temperature

For heat transmission calculations, it is convenient to combine the effects of outdoor air temperature and solar radiation intensity into a single quantity called sol–air temperature. This physical quantity can be expressed as [32, 33]:

$$T_{ea} = T_{air} + \alpha_s G_i/h_0 \quad (23)$$

where T_{ea} is the sol–air temperature (°C), T_{air} is the temperature of the outdoor air (°C), α_s is the solar absorptivity (generally 0.55 for ordinary concrete), and h_0 is the convection heat transfer coefficient (W m^{-2} °C).

Mechanical properties of concrete

Elastic modulus

Elastic modulus of hardened concrete is mainly influenced by the age and temperature. The mathematic model presented by CEB-FIP 1990 code is considered as a convenient and practical way to find the modulus [34, 35]:

$$E_t(t_e) = E_{t28} \times \left\{\exp\left[s \times \left(1 - \sqrt{\frac{28}{t_e - t_s}}\right)\right]\right\}^{nE} \quad (24)$$

where $E_t(t_e)$ is the elastic modulus of early age concrete (MPa) at equivalent age t_e (day), E_{t28} is the elastic modulus of concrete at 28 days cured at 20 °C, t_s is a parameter adjusted to take into account different setting times due to different mix temperatures caused by the use of retarding/accelerating admixtures, and s and nE are two constants determined by the experiments.

Tensile strength

The development of tensile strength is similar to the development of elastic modulus. The formula based on the CEB-FIP code is:

$$f_t(t_e) = f_{t28} \times \left\{ \exp\left[s \times \left(1 - \sqrt{\frac{28}{t_e - t_s}} \right) \right] \right\}^{nt} \quad (25)$$

where $f_t(t_e)$ is the tensile strength of early age concrete (MPa) at equivalent age t_e (day), f_{t28} is the tensile strength of concrete at 28 days cured at 20 °C, and nt is a constant determined from experiments.

Shrinkage effect

Shrinkage of concrete is a time-dependent strain measured in an unloaded and unrestrained specimen at a constant temperature. Shrinkage is generally constituted by autogenous shrinkage, drying shrinkage, and thermal shrinkage at early age [36, 37]. The method of ACI code [10] allows a prediction of the development of shrinkage strain over time as well as a prediction of the final shrinkage strain. According to this method, the final shrinkage strain may be estimated by:

$$\varepsilon_{shu} = 780 \times 10^{-6} \times \gamma_{sh} \quad (26)$$

where ε_{shu} is the ultimate shrinkage strain, and γ_{sh} is the overall coefficients taking into account the effects of curing periods, relative humidity, average thickness of member, slump of fresh concrete, content of fine aggregates, cement content, and air content. Especially, the differential drying shrinkage is also treated as uniform shrinkage in this user-developed program by volume–surface ratio method which is presented by ACI code [10]. The development of shrinkage strain may be expressed by:

$$\varepsilon_{sh} = \frac{t}{35 + t} \varepsilon_{shu} \quad (27)$$

where ε_{sh} is the shrinkage strain at hydration age t which is expressed in days. All these parameters should be acquired from tests to ensure the accuracy for the particular concrete materials.

Creep effect

Mathematical models have been widely used to facilitate a structural analysis involving creep effect of concrete. Several practical models for predicting creep properties for a particular concrete and environmental condition have been developed, such as Bazant–Panula's models, RILEM Model B3, CEB-FIP Model, ACI 209, BS 8110, and Rusch–Jungwirth method.

Creep effect is a nonlinear and time-dependent slow process happened in concrete structures. Using a finite element program, the nonlinear process is simulated by a step-by-step incremental method which needs to store huge data of stress history in a large-scale 3D model. Zhu [38, 39] proposed an implicit method for the creep stress analysis which avoids storing the entire stress history and makes the implementation more feasible. This method is applied in this study.

The creep effect can be fully characterized by the compliance function, $J(t, \tau)$, which represents the total strain at time t produced by a unit constant stress that has been acting since time τ. It is expressed as [40]:

$$J(t, \tau) = \frac{1}{E(\tau)} + C(t, \tau) = \frac{1 + \phi(t, \tau)}{E(\tau)} \quad (28)$$

where $1/E(\tau)$ represents the instantaneous elastic deformation at age τ, $C(t, \tau)$ is the creep compliance, and $\phi(t, \tau)$ is the creep coefficient which is defined as the ratio of the creep deformation to the elastic deformation. The creep compliance can be expressed approximately as [39]:

$$C(t, \tau) = \sum_{r=1}^{3} \phi_r(\tau)[1 - \exp(-S_r \cdot (t - \tau))] \quad (29)$$

where

$$\phi_1(\tau) = A_1 + B_1 \tau^{-G_1}$$
$$\phi_2(\tau) = A_2 + B_2 \tau^{-G_2}$$
$$\phi_3(\tau) = D e^{-S_3 \tau}$$

in which constants A_1, A_2, B_1, B_2, G_1, G_2, S_1, S_2, S_3, and D are determined by experiments on the concrete material used in the structure.

Cracking risk

Cracking risk can be defined as the ratio of the principal tensile stress to the tensile strength [41]:

$$\eta = \frac{\sigma_1(t)}{f_t(t)} \quad (30)$$

where η is the cracking risk, $\sigma_1(t)$ and $f_t(t)$ is the first principal tensile stress and the tensile strength at time t, respectively.

Three-dimensional FEM analysis

Strain analysis

The total incremental strain at the nth time interval is the summation of the incremental strains due to different effects:

$$\{\Delta\varepsilon_n\} = \{\Delta\varepsilon_n^{\mathrm{e}}\} + \{\Delta\varepsilon_n^{\mathrm{cr}}\} + \{\Delta\varepsilon_n^{\mathrm{th}}\} + \{\Delta\varepsilon_n^{\mathrm{sh}}\} \tag{31}$$

where $\{\Delta\varepsilon_n\}$ is the total incremental strain, and $\{\Delta\varepsilon_n^{\mathrm{e}}\}$, $\{\Delta\varepsilon_n^{\mathrm{cr}}\}$, $\{\Delta\varepsilon_n^{\mathrm{th}}\}$, $\{\Delta\varepsilon_n^{\mathrm{sh}}\}$ are the increments of elastic strain, creep strain, thermal strain, and shrinkage strain, respectively. The elastic strain and creep strain are stress-dependent, while the thermal strain and shrinkage strain are stress-independent. In the 3D space, each incremental strain is a column matrix with six components in the form of $[\varepsilon_x \quad \varepsilon_y \quad \varepsilon_z \quad \gamma_{xy} \quad \gamma_{yz} \quad \gamma_{zx}]^T$, where γ_{xy}, γ_{yz}, and γ_{zx} represent engineering shear strains.

Elastic strain

According to the Hooke law, elastic strain increment in the nth time interval, $\Delta\tau_n$, can be expressed as:

$$\{\Delta\varepsilon_n^{\mathrm{e}}\} = \frac{1}{E_n(\tau)}[Q]\{\Delta\sigma_n\} \tag{32}$$

where $E_n(\tau)$ is the elastic modulus which is a function of concrete age τ, $\frac{1}{E_n(\tau)}[Q]$ is the elastic compliance matrix, and $[Q]$ is a matrix in terms of Poisson's ratio μ:

$$[Q] = \begin{bmatrix} 1 & -\mu & -\mu & 0 & 0 & 0 \\ & 1 & -\mu & 0 & 0 & 0 \\ & & 1 & 0 & 0 & 0 \\ & & & 2(1+\mu) & 0 & 0 \\ & \text{sym.} & & & 2(1+\mu) & 0 \\ & & & & & 2(1+\mu) \end{bmatrix}$$

Based on experimental observations, it can be assumed that μ does not vary with the age of concrete τ. Incremental stress $\{\Delta\sigma_n\}$ is a column matrix with six components in the form of $[\sigma_x \quad \sigma_y \quad \sigma_z \quad \tau_{xy} \quad \tau_{yz} \quad \tau_{zx}]^T$.

Creep strain

Creep is a nonlinear time-dependent behavior and is related to its stress history. As a result, the incremental method is used to compute the creep strain by dividing the duration into a set of time intervals. The superposition principal is applied to find the deformation response of all the load increments. For the small increments in stress vector during t_0 to t measured from the setting time, the creep strain in one dimension can be expressed as [39]:

$$\varepsilon^{\mathrm{cr}}(t) = \Delta\sigma_0\, C(t,\, t_0) + \int_{t_0}^{t} C(t,\, \tau)\frac{\mathrm{d}\sigma(\tau)}{\mathrm{d}\tau}\mathrm{d}\tau \tag{33}$$

where $\Delta\sigma_0$ is the stress increment when $t = t_0$, which is the time when the stress increment begins to act and $C(t,\, \tau)$ is the creep compliance defined in Eq. 29. It is known that the Poisson's ratio of concrete can be assumed as a constant and the concrete is considered to be an isotropic material. Thus, in 3D space, the creep strain is presented by:

$$\{\varepsilon^{\mathrm{cr}}(t)\} = [Q]\{\Delta\sigma_0\}C(t,\, t_0) + \int_{t_0}^{t} C(t,\, \tau)[Q]\left\{\frac{\mathrm{d}\sigma(\tau)}{\mathrm{d}\tau}\right\}\mathrm{d}\tau \tag{34}$$

In one typical incremental step, the creep strain can be written as:

$$\{\Delta\varepsilon_n^{\mathrm{cr}}\} = \{\varepsilon^{\mathrm{cr}}(t_n)\} - \{\varepsilon^{\mathrm{cr}}(t_{n-1})\} = \{\eta_n\} + q_n[Q]\{\Delta\sigma_n\} \tag{35}$$

where

$$\{\eta_n\} = [\eta_x \quad \eta_y \quad \eta_z \quad \eta_{xy} \quad \eta_{yz} \quad \eta_{zx}]_n^T = \sum_{r=1}^{3}(1 - \exp(-S_r\,\Delta\tau_n))\{\omega_{r,n}\} \tag{36}$$

$$\{\omega_{r,\,n}\} = [\omega_x\omega_y\omega_z\omega_{xy}\omega_{yz}\omega_{zx}]_{r,n}^T = \{\omega_{r,\,n-1}\} \times \exp(-S_r\,\Delta\tau_{n-1}) + [Q]\{\Delta\sigma_{n-1}\}\phi_{r,n-1}^* f_{r,\,n-1} \times \exp(-S_r\,\Delta\tau_{n-1}) \tag{37}$$

$$\{\omega_{r,\,1}\} = [Q]\{\Delta\sigma_0\}\phi_r(t_0) \tag{38}$$

$$\Delta\tau_n = t_n - t_{n-1} \tag{39}$$

$$q_n = \sum_{r=1}^{3}\phi_{r,n}^* h_{r,\,n}\begin{cases} \phi_{r,n}^* = \phi_r(t_{n-1} + \Delta\tau_n/2) \\ h_{r,n} = 1 - f_{r,n}\exp(-S_r\,\Delta\tau_n) \\ f_{r,n} = [\exp(S_r\,\Delta\tau_n - 1)/S_r]\,\Delta\tau_n \end{cases} \tag{40}$$

S_r and ϕ_r are defined in Eq. 29 for the derivation of the above formulation.

Thermal strain

The thermal strain increment is determined by the coefficient of thermal expansion and the temperature difference:

$$\{\Delta\varepsilon_n^{\mathrm{th}}\} = [\alpha_{\mathrm{th}}\Delta T_n \quad \alpha_{\mathrm{th}}\Delta T_n \quad \alpha_{\mathrm{th}}\Delta T_n \quad 0 \quad 0 \quad 0]^T \tag{41}$$

where α_{th} is the coefficient of thermal expansion, and ΔT_n is the temperature change during $\Delta\tau_n$.

Shrinkage strain

In order to simplify the computation, the shrinkage in the concrete structure is assumed to be uniform and isotropic. The shrinkage deformation can thus be treated similar to thermal expansion which is expressed as:

$$\begin{aligned}\{\Delta\varepsilon_n^{\mathrm{sh}}\} &= \begin{bmatrix}\Delta\varepsilon_n^{\mathrm{sh}} & \Delta\varepsilon_n^{\mathrm{sh}} & \Delta\varepsilon_n^{\mathrm{sh}} & 0 & 0 & 0\end{bmatrix}^T \\ &= \begin{bmatrix}\alpha_{\mathrm{th}}\Delta T_n^{\mathrm{sh}} & \alpha_{\mathrm{th}}\Delta T_n^{\mathrm{sh}} & \alpha_{\mathrm{th}}\Delta T_n^{\mathrm{sh}} & 0 & 0 & 0\end{bmatrix}^T\end{aligned} \tag{42}$$

where $\alpha_{\mathrm{th}}\Delta T_n^{\mathrm{sh}}$ is the equivalent thermal strain corresponding to the shrinkage deformation.

Stress analysis

Based on Eq. 31, the incremental stress can be expressed as

$$\begin{aligned}\{\Delta\sigma_n\} &= [D_n]\{\Delta\varepsilon_n^{\mathrm{e}}\} \\ &= [D_n]\left[\{\Delta\varepsilon_n\} - \{\Delta\varepsilon_n^{\mathrm{cr}}\} - \{\Delta\varepsilon_n^{\mathrm{th}}\} - \{\Delta\varepsilon_n^{\mathrm{sh}}\}\right]\end{aligned} \tag{43}$$

where $[D_n]$ is the elastic material stiffness matrix of the Hooke's law. From the geometric relationship and the shape functions used in the finite element method, it is known that

$$\{\Delta\varepsilon_n\} = [B]\{\Delta\delta_n\} \tag{44}$$

where $[B]$ is equal to the product of the differential operator matrix and the shape function matrix, and $\{\Delta\delta_n\}$ is the incremental nodal displacements at the nth step. Substituting Eqs. 35 and 44 into Eq. 43, the incremental stress can be rewritten as:

$$\{\Delta\sigma_n\} = \overline{[D_n]}\left([B]\{\Delta\delta_n\} - \{\eta_n\} - \{\Delta\varepsilon_n^{\mathrm{th}}\} - \{\Delta\varepsilon_n^{\mathrm{sh}}\}\right) \tag{45}$$

$$\overline{[D_n]} = \left([I] + q_n[D_n][Q]\right)^{-1}[D_n] = [D_n]/(1 + q_n E_n). \tag{46}$$

In the finite element method, the governing equation can finally be converted to

$$\int [B]^T\{\Delta\sigma_n\}\mathrm{d}V = \{\Delta R_n\} \tag{47}$$

where $\{\Delta R_n\}$ is the incremental equivalent nodal forces. Substitution of Eq. 45 into Eq. 47 yields:

$$\begin{aligned}[K]\{\Delta\delta_n\} &= \{\Delta R_n\} + \{\Delta R_n^{\mathrm{cr}}\} + \{\Delta R_n^{\mathrm{th}}\} + \{\Delta R_n^{\mathrm{sh}}\} \\ \{\Delta R_n^{\mathrm{cr}}\} &= \int [B]\overline{[D_n]}\{\eta_n\}\mathrm{d}V \\ \{\Delta R_n^{\mathrm{th}}\} &= \int [B]\overline{[D_n]}\{\Delta\varepsilon_n^{\mathrm{th}}\}\mathrm{d}V \\ \{\Delta R_n^{\mathrm{sh}}\} &= \int [B]\overline{[D_n]}\{\Delta\varepsilon_n^{\mathrm{sh}}\}\mathrm{d}V\end{aligned} \tag{48}$$

where $[K]$ is the stiffness matrix which is calculated by $\int [B]^T[\bar{D}][B]\mathrm{d}V$, $\{\Delta R_n^{\mathrm{cr}}\}$, $\{\Delta R_n^{\mathrm{th}}\}$, and $\{\Delta R_n^{\mathrm{sh}}\}$ are the incremental equivalent nodal forces due to creep, thermal, and shrinkage, respectively. By solving Eq. 48, incremental displacement vector $\{\Delta\delta_n\}$ can be calculated and then $\{\Delta\sigma_n\}$ can be obtained from Eqs. 43 and 44. The total stress at the nth step is $\{\sigma_n\} = \{\sigma_{n-1}\} + \{\Delta\sigma_n\}$.

Governing equation of heat conduction for concrete

At the early age, a great deal of heat is released from the hydration of cement and causes temperature increasing in the concrete. This heat conduction problem of hydration effect can be modeled using a diffusion equation in the following form:

$$\begin{aligned}&\frac{\partial}{\partial x}\left(k_x(\alpha(t_{\mathrm{e}}))\frac{\partial T}{\partial x}\right) + \frac{\partial}{\partial y}\left(k_y(\alpha(t_{\mathrm{e}}))\frac{\partial T}{\partial y}\right) + \frac{\partial}{\partial z}\left(k_z(\alpha(t_{\mathrm{e}}))\frac{\partial T}{\partial z}\right) \\ &\quad + \rho c(\alpha(t_{\mathrm{e}}))\frac{\partial\theta(t_{\mathrm{e}})}{\partial t} = \rho c(\alpha(t_{\mathrm{e}}))\frac{\partial T}{\partial t}\end{aligned} \tag{49}$$

where T is the temperature in concrete (°C), θ is the adiabatic temperature rise (°C), k_x, k_y, k_z are the thermal conductivity (W m^{-1} °C), and c is the specific heat (kJ kg^{-1} °C) varying with the degree of hydration α as stated previously. For a given concrete structure, three types of boundary conditions are possible:

$$\text{on boundary } S_1 : T(x, y, z, t) = T_0 = \text{const.}$$

$$\begin{aligned}\text{on boundary } S_2 : &-\left(k_x\frac{\partial T}{\partial x}n_x + k_y\frac{\partial T}{\partial y}n_y + k_z\frac{\partial T}{\partial z}n_z\right) \\ &= q_{\mathrm{c}} + q_{\mathrm{r}} + q_{\mathrm{s}}\end{aligned}$$

$$\begin{aligned}\text{on boundary } S_3 : &-\left(k_x\frac{\partial T}{\partial x}n_x + k_y\frac{\partial T}{\partial y}n_y + k_z\frac{\partial T}{\partial z}n_z\right) \\ &= h_{\mathrm{c}}(T - T_{\mathrm{amb}})\end{aligned}$$

where q_{c}, q_{r}, and q_{s} are the heat flux of air convection, thermal radiation, and solar radiation, respectively (W m^{-2}), n_x, n_y, and n_z are the x, y, z components of the unit outward normal to the surface, respectively, T_{amb} is the ambient temperature (°C), and h_{c} is the heat transfer coefficient between the concrete surface and the surrounding air (W m^{-1} °C).

Simulation process and results

The three-dimensional simulation of thermal stress for early age concrete is divided into two parts. First, a thermal analysis is carried out to compute the temperature field in the concrete. Second, a stress-field analysis is performed using the results obtained from the thermal analysis. The mechanical properties of concrete which vary with the age and the temperature in the concrete are calculated at each time increment of the stress analysis.

Calculation of temperature field

For the calculation of the temperature field, the heat generated in the hardening process of concrete, the thermal

properties of concrete based on degree of hydration, and the effect of the solar radiation and the ambient air temperature on the boundary condition of hardening concrete have been introduced in the Mathematic Models mentioned at the beginning of this article. The flow chart of the finite element analysis for the calculation of temperature field is given in Fig. 1.

The 3D thermal solid element SOLID70 in ANSYS is used for the finite element analysis. To solve the governing equation of Eq. 49 with the development of specific heat and thermal conductivity as shown in Eq. 7, the specified duration of the analysis is divided into many small time steps with iterations in each step to simulate the nonlinear behavior. The numerical algorithm is described as follows:

(1) Input the initial material properties and the boundary conditions. Also input the temperature field T_0 at the beginning of the 1st time step at all the nodes of the finite element mesh. The temperature field at the beginning and at the end of the ith time step is represented by T_{i-1} and T_i, respectively;

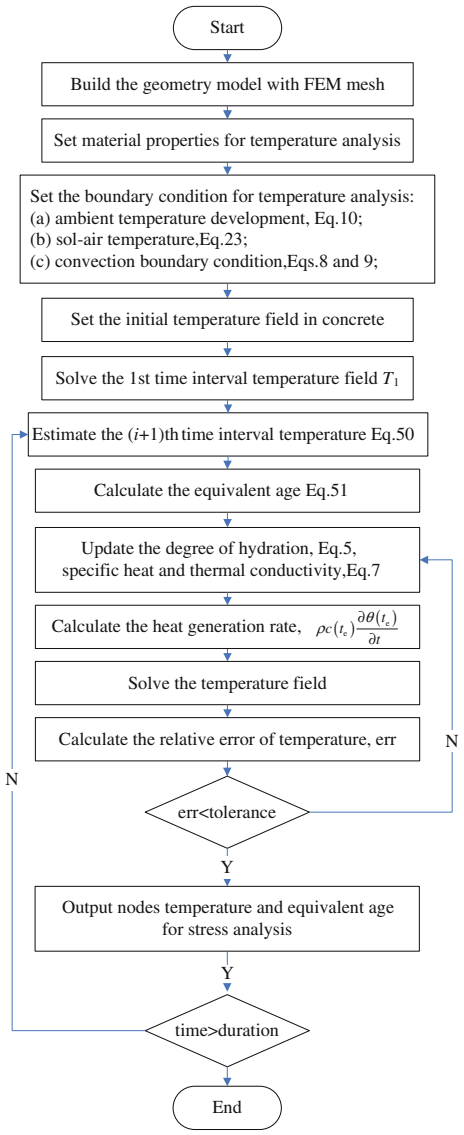

Fig. 1 Flow chart for FEM temperature analysis

(2) Solve the governing equation based on the given initial material properties and boundary conditions to get the temperature field T_1 at the end of the 1st time step;

(3) For the 1st iteration in the $(i + 1)$th time step, the estimated temperature of each node $T_{i+1}^{(0)}$ at the end of the iteration is obtained by assuming linear variation during the time interval:

$$T_{i+1}^{(0)} = T_i + \frac{T_i - T_{i-1}}{t_i - t_{i-1}}\Delta t_{i+1} \tag{50}$$

where the subscript indicates the number of iterations, and superscript (0) here represents the initial estimated temperature at the 1st iteration, Δt_{i+1} is the duration in the $(i + 1)$th time step, and $t_{i+1} = -t_i + \Delta t_{i+1}$ is the accumulated time at the end of the $(i + 1)$th time step;

(4) Use Eq. 4 to calculate the equivalent age $t_{e,i+1}$. Assuming the exponential term in Eq. 4 varies linearly within the time interval, the incremental equivalent age can be expressed as:

$$\Delta t_{e,i+1} = \frac{1}{2}\left[\frac{E_a}{R}\exp\left(\frac{1}{293} - \frac{1}{273 + T_i}\right) + \frac{E_a}{R}\exp\left(\frac{1}{293} - \frac{1}{273 + T_{i+1}}\right)\right]\Delta t_{i+1} \tag{51}$$

The equivalent age $t_{e,i+1}$ equal to $t_{e,i} + \Delta t_{e,i+1}$;

(5) Update the degree of hydration $\alpha(t_e)$ based on Eq. 5 and then re-calculates the specific heat $c(\alpha)$ and thermal conductivity $k(\alpha)$ using Eq. 7;

(6) Calculate the heat generation rate $\rho c(\alpha)\left(\frac{\partial\theta(t_e)}{\partial t}\right)$, which appears in the governing equation, Eq. 49, in the small time interval Δt_{i+1} by approximating $\frac{\partial\theta(t_e)}{\partial t}$ with $\frac{\Delta\theta_{i+1}}{\Delta t_{i+1}}$;

(7) Solve the governing equation based on the updated material properties to find the temperature field $T_{i+1}^{(k)}$ at the kth iteration in the $(i + 1)$th time step;

(8) Calculate the norm of relative errors $\left|\frac{T_{i+1}^{(k)} - T_{i+1}^{(k-1)}}{T_{i+1}^{(k)}}\right|$ in the kth iteration. If the relative error is higher than a given tolerance which depends on the required accuracy, go to step (5) for the next iteration and use temperature field $T_{i+1}^{(k)}$ to update the material properties during the new iteration. If the error is less than the given tolerance, stop the iteration and go to step (3) for the next time step.

Calculation of thermal stress field

Stress fields are calculated by taking into account the thermal, creep, and shrinkage effects as shown in Eq. 48. The finite element program ANSYS provides UPFs and ANSYS Parametric Design Language (APDL) to let users be able to define a new material model, add a special element, or modify a failure criterion. In ANSYS program, the material user subroutine USERMAT.F defines the stress–strain constitutive law based on the stress state in the material. This subroutine calls another four subroutines USERMAT3D.F, USERMATPS.F, USERMATBM.F, and USERMAT1D.F, each of which can be used as a user-defined material constitutive law for a specific element. In this study, based on the subroutine USERMAT3D.F and element type SOLID185 provided by ANSYS program, a new subroutine for the new material constitutive law was developed to describe the early age concrete behaviors including the creep effect, shrinkage strains, thermal strains, and the development of the age-dependent elastic modulus.

The user-defined USERMAT3D.F is compiled into the ANSYS program to simulate the behavior of early age concrete. The flow chat for the stress analysis is given in Fig. 2. A step-by-step implicit time integration method is used in this finite element analysis because of the nonlinear characteristics of the behavior with time-dependent thermomechanical properties.

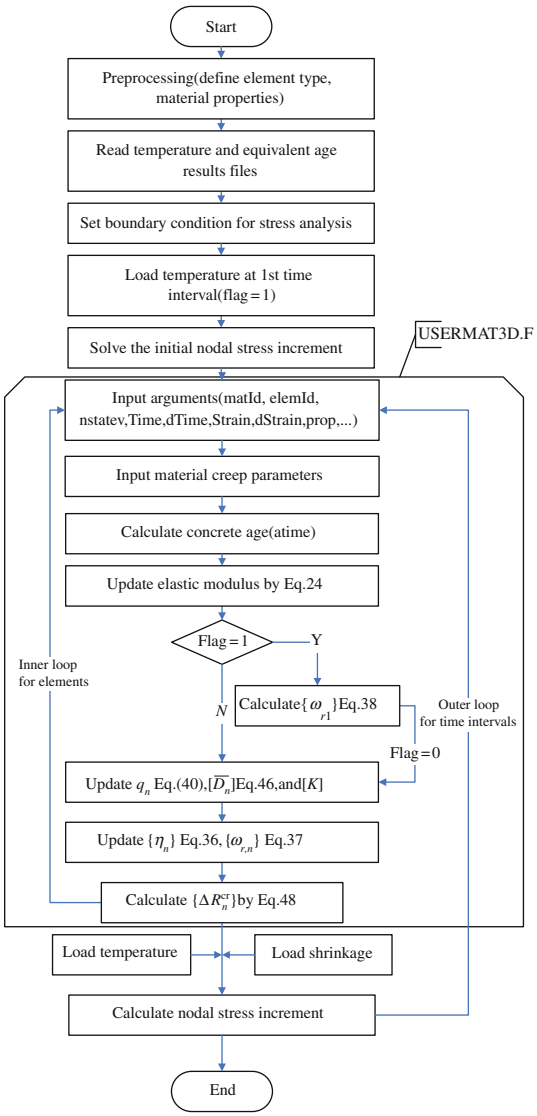

Fig. 2 Flow chart for FEM stress analysis

Model validation based on the field tests

The calculations on the structure of Maridal culvert in Norway presented in Fig. 3a were performed with the FE model shown as Fig. 3b in which the material and environmental parameters were provided or deduced from the field tests presented by the report [42]. Figures 4 and 5 illustrate the temperature and stress variations for the top and bottom parts in the wall between the calculation results and field test data which are referenced from [28, 42, 43]. It can be seen that the simulation results agree well with the filed test results, which proves that the user-developed program is effective.

Parametric studies

In this part, the calibrated FE model is used to perform parametric studies to evaluate the effect of hydration heat, ambient temperature and casting temperature on temperature variations, and crack behavior of early age concrete. It is considered that the simulation case is happened in summer (July 30) under the hot weather. The wall is supposed to lie in the north–south direction so that the wall has large surfaces exposed to the sunlight. The main input parameters are summarized in Table 1 including solar radiation, material properties, and boundary conditions.

According to a good many simulation results and observed field phenomena, we know that the stress in the lower part of wall close to the foundation is expected the place where the maximum stress occurs. For instance, Larson [28] showed the observed cracking of the similar structure was located at the bottom of the wall. Lee [44] predicted typical early age cracking due to edge restraint for concrete slab, and the crack mainly occurs just above the interface between wall and foundation. Therefore, the interested points in this analysis are located also in the lower part of the wall. The surface point is marked as 'SP' and the internal point is marked as 'IP', which are located at the middle section of the wall shown as Fig. 3c.

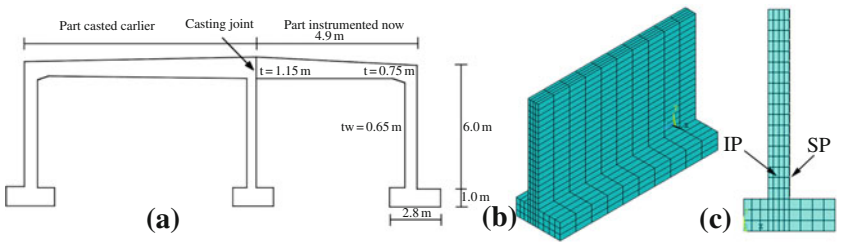

Fig. 3 **a** Maridal culvert geometry [43], **b** FE model mesh of wall, and **c** interested points in middle section

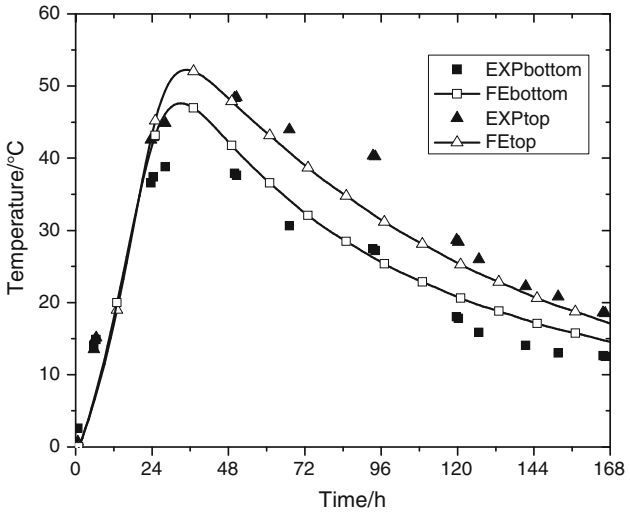

Fig. 4 The comparisons of temperature variations for top and bottom points in the wall between experimental and calculation results

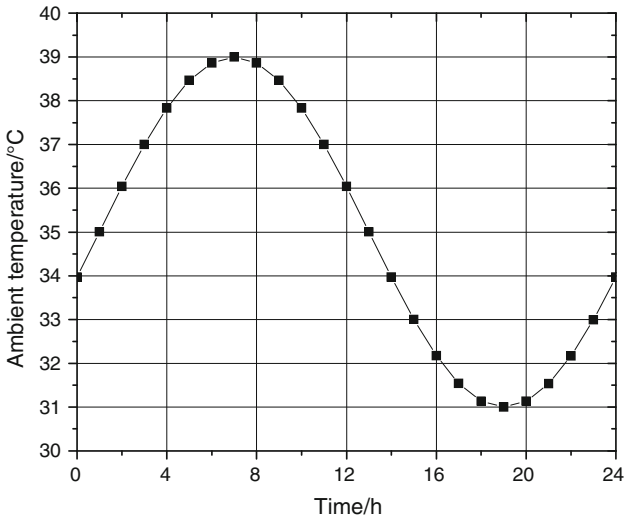

Fig. 6 Supposed daily ambient temperature on July 30

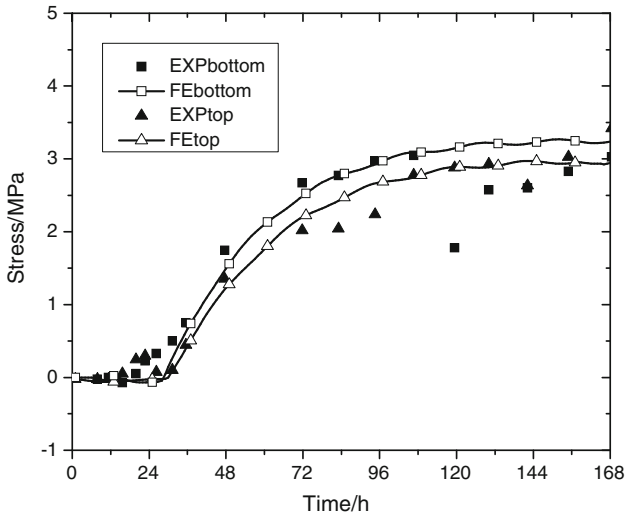

Fig. 5 The comparisons of stress variations for top and bottom points in the wall between experimental and calculation results

Effect of hydration heat

In early age concrete structures, the hydration heat plays an important role in the stress development due to its significant effect on the temperature development. The temperature rise caused by cement hydration may make great temperature differences between the center and the surface of the concrete wall, which enlarges the cracking risk that can be calculated by Eq. 30. The cracking risk developments of surface and internal of concrete wall were shown in Figs. 7 and 8, respectively, in which three different ultimate adiabatic temperature rises are considered including 37, 43.5, and 50 °C based on Eq. 6. It is worth to notice that the cracking risk increases with the increasing ultimate adiabatic temperature rise, particularly, in the center of the wall. That means the lower heat of hydration generates, the lower cracking risk will occur in the hot weather.

Effect of ambient temperature

Besides the hydration heat, ambient temperature also changes the temperature distributions in the concrete construction. Especially in different seasons, the daily ambient temperature changes a lot with the sol–air temperature. The ambient temperature is dependent on the air temperature and the solar irradiation. Figure 9 shows the one-day ambient temperature in different

Table 1 Main input parameters for FE model

Parameters	Values	Note
Adiabatic temperature rise	$\theta_u = 43.5/°C$, $\xi = -1.3$	Eq. 6
Ambient temperature	Shown in Fig. 6	Eq. 10
Removal of formwork	After 24 h	
Thermal conductivity of formwork	0.17/W m^{-1} °C (wood)	Constant
Wind velocity	2.0/m s^{-1}	Eq. 9
Density	2400/kg m^{-3}	Constant
Coefficient of thermal expansion	$10^{-5}/°C^{-1}$	Constant
Poison ratio	0.167	Constant
Specific heat	$c_0 = 0.9$/kJ kg^{-1}	Eq. 7
Thermal conductivity	$k_0 = 2.7$/W $m^{-1}°C$	Eq. 7
Elastic modulus	$E_{r28} = 42.5$/GPa, $s = 0.21$, $t_0 = 5$, $nE = 0.447$	Eq. 24
Tensile strength	$f_{r28} = 2.8$/MPa, $s = 0.21$, $t_0 = 5$, $nt = 0.573$	Eq. 25
Shrinkage	$-780 \times (t/(35 + t))$ (10^{-6})	Eqs. 26 and 27
Creep	$A_1 = 0.23/(1.5E_{r28})$, $B_1 = 2.67/(1.5E_{r28})$, $G_1 = 0.45$, $S_1 = 0.3$; $A_2 = 0.52/(1.5E_{r28})$, $B_2 = 0.88/(1.5E_{r28})$, $G_2 = 0.45$, $S_2 = 0.005$; $D = 0$	Eqs. 28 and 29

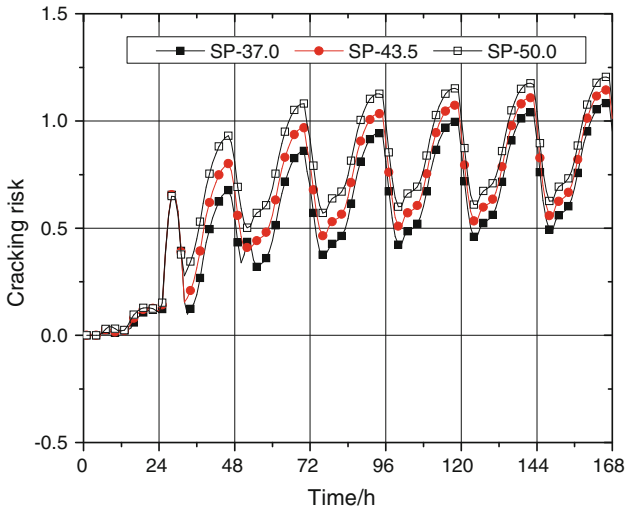

Fig. 7 Effect of hydration heat on cracking risk on the surface of concrete wall

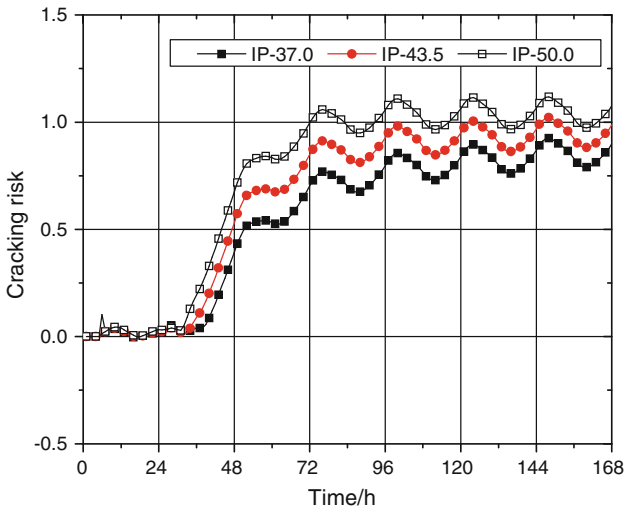

Fig. 8 Effect of hydration heat on cracking risk in the central of concrete wall

seasons. According to Eqs. 18 and 19, the corresponding solar beam irradiation (Gb) and diffuse irradiation (Gd) is shown in Fig. 10.

The effects of the ambient temperature on the cracking risk are given in Figs. 11 and 12. It indicates that the cracking risk both on surface and in the wall will decrease dramatically if the concrete wall is built in March or December when the other conditions keep the same.

Effect of casting temperature

The concrete casting temperature plays a significant role during concrete casting and curing period. Higher temperatures speed up the hydration reaction, while lower temperatures slow it down. Figures 13 and 14 show the effect of casting temperature on cracking risk on the surface and in the center of the concrete wall, respectively. It is seen that the lower casting temperature reduces the

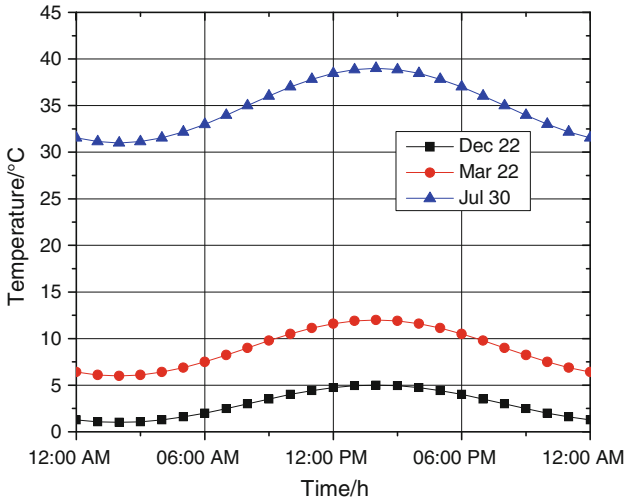

Fig. 9 Ambient temperature on Dec 22, Mar 22, and Jul 30

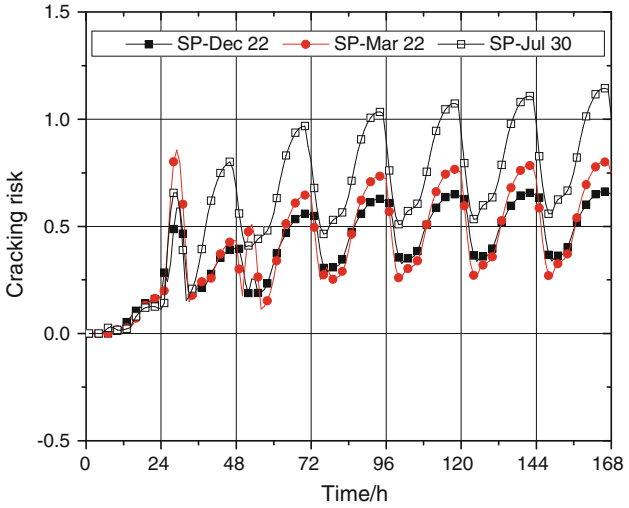

Fig. 11 Effect of ambient temperature on cracking risk on the surface of concrete wall

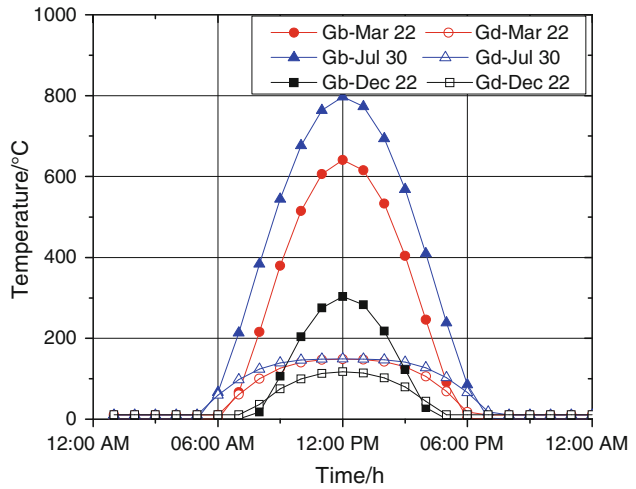

Fig. 10 Solar beam radiation and diffuse radiation on Dec 22, Mar 22, and Jul 30

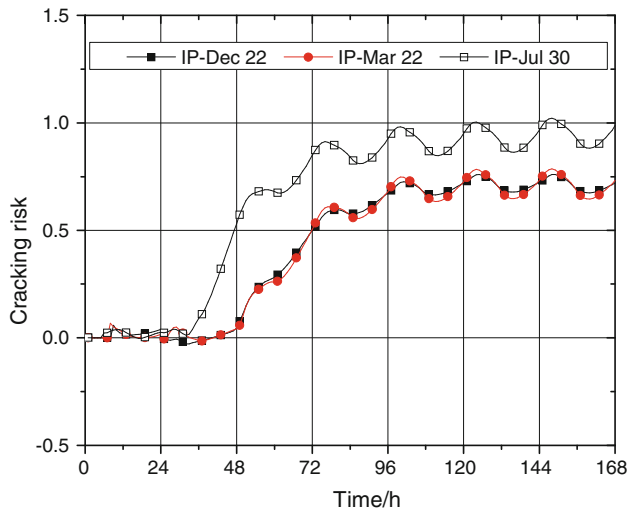

Fig. 12 Effect of ambient temperature on cracking risk in the center of concrete wall

cracking risk, especially, in the center of the wall. It is suggested that dropping casting temperature is a good method to avoid the cracks in hot weather.

Effect of wind velocity

Since the concrete is generally exposed outdoors, the wind will go over the construction. During the hardening process of concrete, the wind will speed up the convection between the concrete and the air which will help the heat loss of concrete. Regarding this issue, three different wind velocities are used to analyze its effect on the cracking risk. From Figs. 15 and 16, it is seen that the high wind velocity will raise the cracking risk during the first 4 days and after that the influence can be ignored.

Effect of uniform shrinkage

When assessing the cracking potential of concrete, it is critical to refer to the total shrinkage including drying shrinkage, autogenous shrinkage, and carbonation shrinkage. Figures 17 and 18 show that the shrinkage has a significant effect on the cracking risk of the hardening concrete.

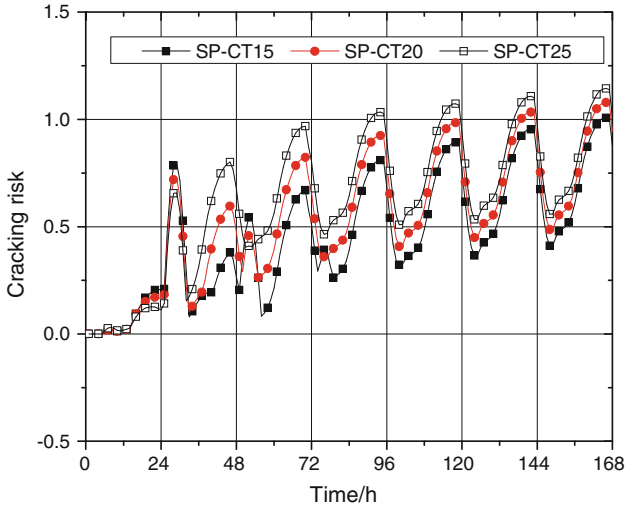

Fig. 13 Effect of casting temperature on cracking risk on the surface of concrete wall

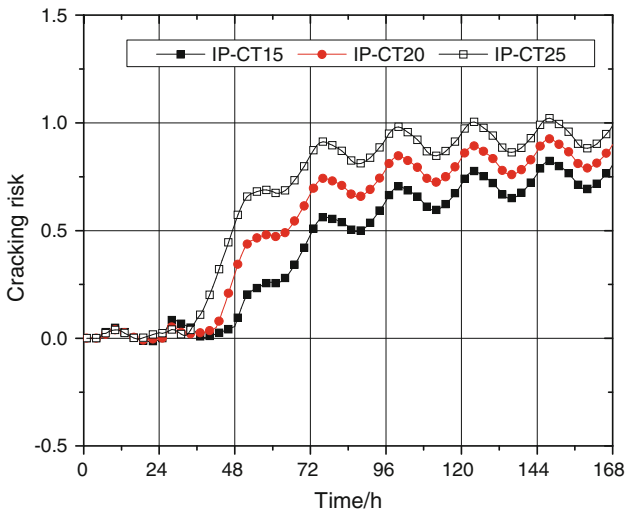

Fig. 14 Effect of casting temperature on cracking risk in the center of concrete wall

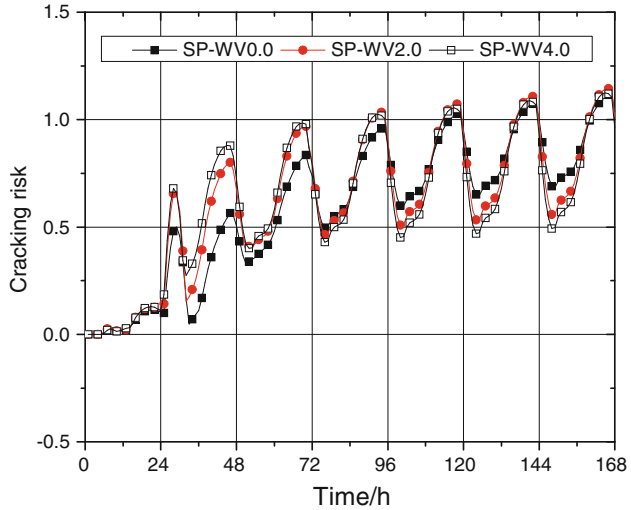

Fig. 15 Effect of wind velocity on cracking risk on the surface of concrete wall

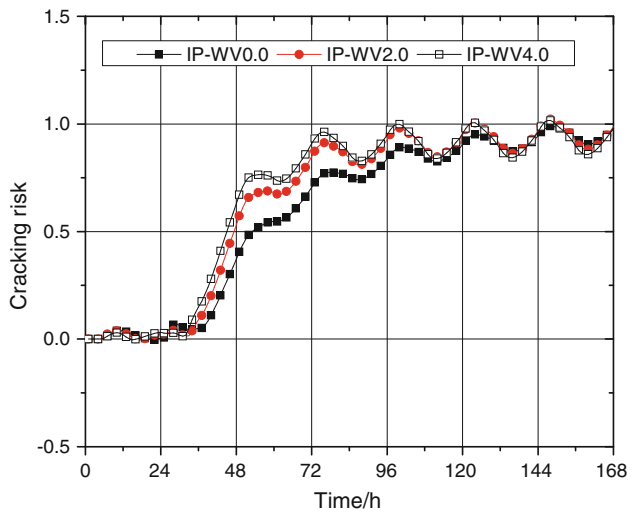

Fig. 16 Effect of wind velocity on cracking risk in the center of concrete wall

The uniform shrinkage increases the cracking possibility of both the surface and the interior of the concrete wall due to the restraint from the hardened concrete in the foundation.

Effect of wall length–height ratio

The length–height ratio (L/H) can be considered as a kind of external restraint. In this analysis, three length–height ratios are considered including 5.0/5.8, 10.0/5.8, and 15.0/5.8 by changing the wall length. The results are shown in Figs. 19 and 20. When the length–height ratio is 5.0/5.8 which is less than 1.0, the cracking risk is reduced obviously which means cracks will not appear during this case. However, when the length–height ratio is greater than 1.0, the cracking risk is going up to and beyond 1.0 which means the cracks will probably happen. It is considered that the larger length–height ratio increases the restrain of hardened concrete foundation on the early age concrete, and results in higher stress.

From the parametric study, the effective measures to control the cracking of concrete at early age are given as follows: reducing the heat release by cementitous, casting the concrete wall in cool weather, dropping the casting temperature, preventing the concrete surface from wind, adopting the expansive cement as the cementitous to

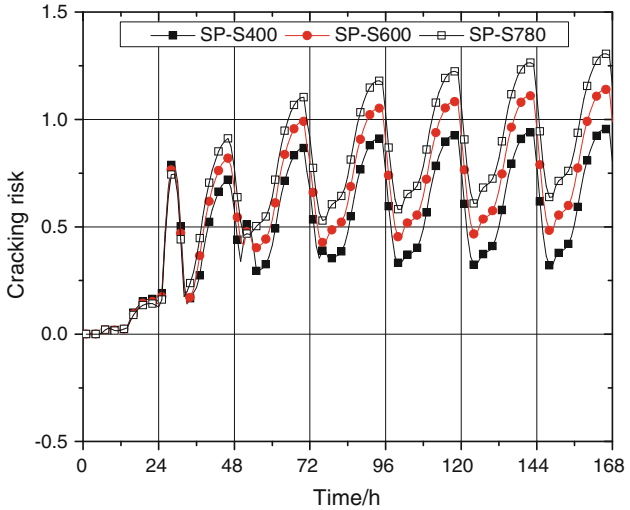

Fig. 17 Effect of uniform shrinkage on cracking risk on the surface of concrete wall

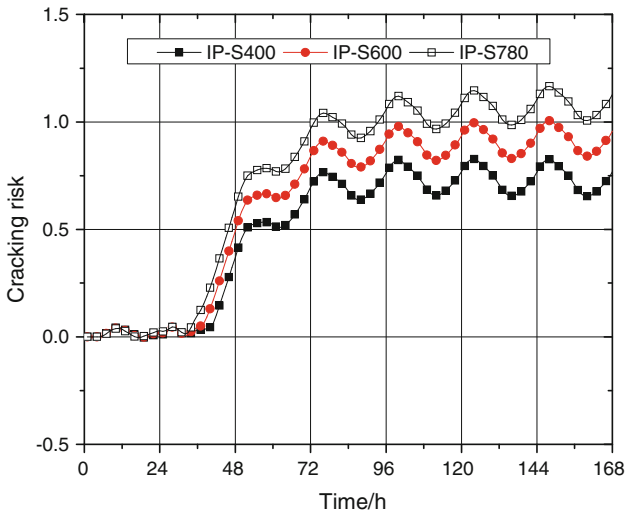

Fig. 18 Effect of uniform shrinkage on cracking risk in the center of concrete wall

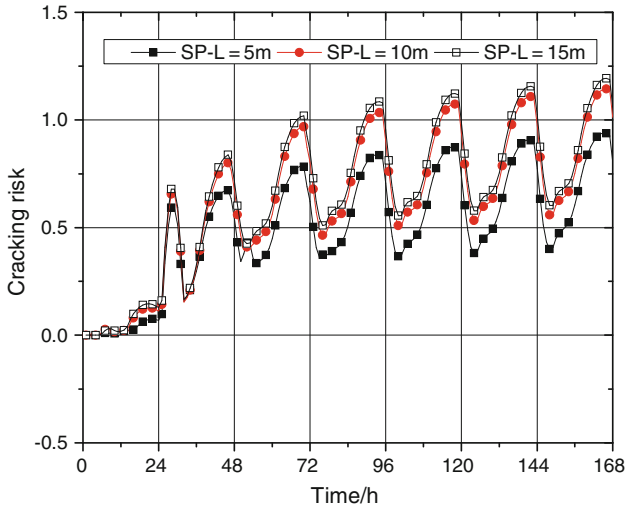

Fig. 19 Effect of *L*/*H* on cracking risk on the surface of concrete wall

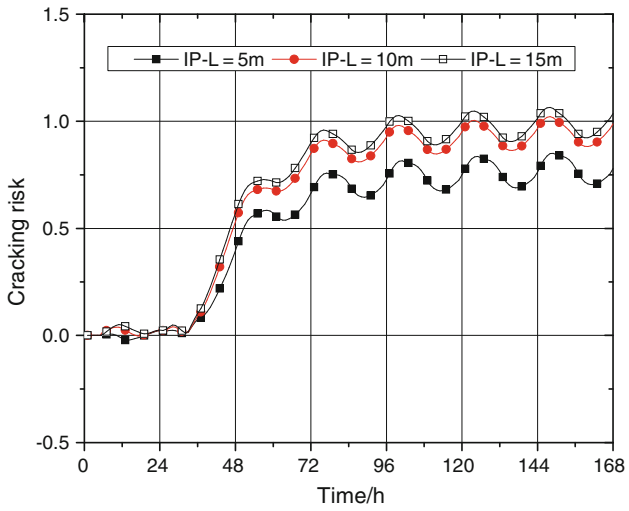

Fig. 20 Effect of *L*/*H* on cracking risk in the center of concrete wall

reduce the shrinkage, and casting the concrete wall part by part in length direction.

Conclusions

Based on 3D finite element method, a user-developed program was carried by the UPFs of ANSYS program considering the development of heat of hydration, elastic modulus, creep, shrinkage, and solar radiation. The temperature and thermal stress analysis were conducted to validate the developed model. The parametric study was carried out by parametric studies to estimate the effect of various factors on the cracking risk. The following contributions were drawn from this study:

(1) A new user-defined subroutine was developed considering the development of material properties of concrete at early age and the environmental conditions. Application to the on-site Maridal culvert in Norway gave results in good agreement with the ones from field tests.

(2) This study indicates that thermal stress in a thick wall is affected by ambient temperature, solar radiation, heat of hydration, and casting temperature of concrete. In particular, ambient temperature affects the stress on the surface of the concrete wall, while heat of hydration and casting temperature play more important roles in the center of the wall. The high

wind velocity raises the cracking risk during the first couple days. The smaller shrinkage reduces the restrain stress. Reducing the length–height ratio is a good way to avoid cracking.

(3) Finally, based on the parametric studies, some measures are provided for preventing the early age concrete from cracking.

Acknowledgements The authors acknowledge the financial support from the National Natural Science Foundation of China (NSFC) under Grant No. 50779017. The authors also want to appreciate the scholarship awarded to the Donghui Huang by the China Scholarship Council during his 1-year study in City College of City University of New York. Dr. Xiaochun Li and Dr. Hongmei Gao are very appreciated for their contribution to this article.

References

1. Kjellman O, Olofsson J. 3D structural analysis of crack risk in hardening concrete structures. Verification of a three-step engineering method; 1999. Contract No.: TG 4/N2.
2. Nocun-Wczelik W, Stok A, Konik Z. Heat evolution in hydrating expansive cement systems. J Therm Anal Calorim. 2010;101: 527–32.
3. Du C, Liu G. Numerical procedure for thermal creep stress in mass concrete structures. Commun Numer Eng. 1994;10(7): 545–54.
4. Bazant ZP. Prediction of concrete creep and shrinkage: past, present and future. Nucl Eng Des. 2001;203(1):27–38.
5. Altoubat SA, Lange DA. Creep, shrinkage, and cracking of restrained concrete at early age. ACI Mater J. 2001;98(4):323–31.
6. De Schutter G. Finite element simulation of thermal cracking in massive hardening concrete elements using degree of hydration based material laws. Comput Struct. 2002;80:2035–42.
7. Yuan Y, Wan ZL. Prediction of cracking within early-age concrete due to thermal, drying and creep behavior. Cem Concr Res. 2002;32(7):1053–9.
8. Wu Y, Luna R. Numerical implementation of temperature and creep in mass concrete. Finite Elem Anal Des. 2001;37(2): 97–106.
9. Amin MN, Kim J-S, Lee Y, Kim J-K. Simulation of the thermal stress in mass concrete using a thermal stress measuring device. Cem Concr Res. 2009;39(3):154–64.
10. ACI209R-92. Prediction of creep, shrinkage, and temperature effects in concrete structures: American Concrete Institute; 1992.
11. van Breugel K, Koenders EAB. Effect on solar radiation on the risk of cracking in young concrete, Delft University of Technology; 2001. Report No.: BE96-3843.
12. Borst RD, Boogaard AH. Finite-element modeling of deformation and cracking in early-age concrete. J Eng Mech. 1994; 120(12):2519–34.
13. Vartiainen E. New approach to estimating the diffuse irradiance on inclined surfaces. Renew Energy. 2000;20(1):45–64.
14. Chwieduk DA. Recommendation on modelling of solar energy incident on a building envelope. Renew Energy. 2009;34(3): 736–41.
15. van Breugel K. Simulation of hydration and formation of structure in hardening cement-based materials. Delft: Delft University of Technology, Doctoral thesis; 1991.
16. Schindler AK, Folliard KJ, editors. Influence of supplementary cementing materials on the heat of hydration of concrete. Advances in Cement and Conrete IX Conference; 2003; Copper Mountain Conference Resort in Colorado.
17. Goni S, Puertas F, Hernandez MS, Palacios M, Guerrero A, Dolado JS, et al. Quantitative study of hydration of C_3S and C_2S by thermal analysis. J Therm Anal Calorim. 2010;102:965–73.
18. Carino NJ, Lew HS, editors. The maturity method: from theory to application. In: Proceedings of the 2001 structures congress & exposition; 2001 May 21–23; Washington, DC: American Society of Civil Engineers.
19. Gruyaert E, Robeyst N, Belie ND. Study of the hydration of Portland cement blended with blast-furnace slag by calorimetry and thermogravimetry. J Therm Anal Calorim. 2010;102:941–51.
20. Dimon P. Material stability predictions applying a new non-arrhenian temperature function. J Therm Anal Calorim. 2009;97: 391–6.
21. Knudsen T, editor. Modeling hydration of Portland cement—the effects of particle size distribution. In: Proceedings of the engineering foundation conference on characterization and performance prediction of cement and concrete; 1982 July; Henniker, NH: United Engineering Trustees Inc.
22. Kjellsen KO, Detwiler RJ. Later-age strength prediction by a modified maturity model. ACI Mater J. 1993;90(3):220–7.
23. McCullough BF, Ransmussen RO. Fast track paving: concrete temperature control and traffic opening criteria for bonded concrete overlays; 1998. U.S.: FHWA1998 Contract No.: Final Report.
24. Ulm F-J, Coussy O. Modeling of thermochemomechanical couplings of concrete at early ages. J Eng Mech. 1995;121(7): 785–94.
25. Nakamura H, Hamada S, Tanimoto T, Miyamoto A. Estimation of thermal crack resistance for mass concrete structures with uncertain material properties. ACI Struct J. 1999;96(4):509–18.
26. Emanuel JH, Hulsey JL. Prediction of the thermal coefficient of expansion of concrete. J ACI. 1977;74(4):149–55.
27. Sellevold EJ, Bjntegaard Ø. Coefficient of thermal expansion of cement paste and concrete: mechanisms of moisture interaction. Mater Struct. 2006;39:809–15.
28. Larson M. Thermal crack estimation in early age concrete-models and methods for practical application. Lulea University of Technology, Doctoral thesis; 2003.
29. Bilbao J, de Miguel AH, Kambezidis HD. Air temperature model evaluation in the north mediterranean belt area. J Appl Meteorol. 2002;41(8):872–84.
30. Spencer JW. Fourier series representation of the position of the sun. Search. 1971;2(5):172.
31. Rigollier C, Bauer O, Wald L. On the clear sky model of the ESRA—European Solar Radiation Atlas—with respect to the heliosat method. Sol Energy. 2000;68(1):33–48.
32. Threlkeld JL. Thermal environmental engineering. New Jersey: Prentice-Hall Inc.; 1970.
33. Kaska O, Yumrutas R, Arpa O. Theoretical and experimental investigation of total equivalent temperature difference (TETD) values for building walls and flat roofs in turkey. Appl Energy. 2009;86(5):737–47.
34. Kanstad T, Hammer TA, Bjntegaard Ø, Sellevold EJ. Mechanical properties of young concrete: part ii: determination of model parameters and test program proposals. Mater Struct. 2003;36(258): 226–30.
35. CEB-FIP model 1990, CEB bulletin No. 203. Lausanne, Switzerland; 1991.
36. Holt E, Leivo M. Cracking risks associated with early age shrinkage. Cem Concr Compos. 2004;26(5):521–30.
37. Lura P, Winnefeld F, Klemm S. Simultaneous measurements of heat of hydration and chemical shrinkage on hardening cement pastes. J Therm Anal Calorim. 2010;101(3):925–32.

38. Zhu BF. Some problems in the theory of creep in concrete. J Hydraul Eng. 1982;3:35–40.
39. Zhu BF. An implicit method for the stress analysis of concrete structures considering the effect of creep. J Hydraul Eng. 1983; 5:40–6.
40. Bazant ZP, Wittmann FH. Creep and shrinkage in concrete structures. Chichester, New York, Brisbane, Toronto, Singapore: Wiley; 1982.
41. Bernander S. Practical measure to avoiding early age thermal cracking in concrete structures. RILEM; 1997. Report No.: TC 119-TCE.
42. Heimdal E, Kanstad T, Kompen R. Maridal cuvert Norway-field tests I: division of Structural Engineering. Lulea University of Technology; 2001. Report No.: BE96-3843.
43. Heimdal E, Kanstad T, Kompen R. Maridal cuvert Norway-field tests II: division of Structural Engineering. Lulea University of Technology; 2001. Report No.: BE96-3843.
44. Lee Y, Kim J-K. Numerical analysis of the early age behavior of concrete structures with a hydration based microplane model. Comput Struct. 2009;87:1085–101.